Contract No:

This document was prepared in conjunction with work accomplished under Contract No. DE-AC09-08SR22470 with the U.S. Department of Energy (DOE) Office of Environmental Management (EM).

Disclaimer:

Synthesis and Characterization of Novel Nanothermometers

Delphine Baumert*[1], George Larsen[1], PhD, Kaitlin Coopersmith[1], PhD, Sarah Schyck[1], Simona Murph[1]**, PhD

[1]Savannah River National Laboratory,

Savannah River Site

Aiken, SC 29803

*Presenter: D. Baumert

**Simona.Murph@srnl.doe.gov

AuNP: Gold Nanoparticle
BP: Base Pair
FRET: Förster Resonance Energy Transfer
LSPR: Localized Surface Plasmon Resonance
MB: Molecular Beacon
NIR: Near Infrared
NP: Nanoparticle
NSET: Nanometal Surface Energy Transfer
NT: Nucleotide
PALS: Phase Analysis Light Scattering
SEM: Scanning Electron Microscope
SL: Stem Loop

Introduction

Nanoparticles have been around since ancient times.[a] For example, a cup manufactured by the Romans in the fourth century appears green under normal conditions, but changes to red when illuminated from the inside.[a,aa] This phenomenon is a result of gold nanoparticles (AuNPs) that were used to color the glass.[a,aa] About 150 years ago, Michael Faraday made one of the first big steps in nanoparticle (NP) research when he studied the interaction of light and metal NPs and realized that colloidal gold solutions do not exhibit the same properties as bulk gold.[a,b,bb] Even today, the main motivation to study metal NPs is a result of their interesting properties that are different than their bulk counterparts. For example, inert materials can become efficient catalysts, insulators can grow highly conductive, and opaque substances can appear transparent.[a] These properties are due to their large surface area to volume ratios.[bb]

In 1996, Mirkin et al. attached a thiol modified DNA to an AuNP surface via an Au-S bond.[d] Two batches of NP-DNA conjugates with non-complementary sequences were combined, and the solution remained red. When a third strand of DNA (that is able to hybridize with the other sequences) was added, the color of the solution immediately changed from red to blue, indicating that that particles agglomerated (Figure κ.).[d] Mirkin's experiment marked the birth of the development of a highly selective colorimetric assay, and was the beginning to a whole new class of medical diagnostics technology.[d],[g,u,v] Since Mirkin's original experiment, many variations have been explored, resulting in a wide variety of applications.[g,u] For example, Rinnan et al. reported that DNA functionalized AuNPs can be used as thermometers to measure temperatures in the range of range of 20-60 °C at micro and nanoscales.[g] Most experiments focus on using AuNPs, so we assessed the potential of other multifunctional NPs, including Au-Fe_2O_3, Pd, Pd-Fe_2O_3 and Au-Pd-Fe_2O_3 NPs as nanothermometers. Our research focuses on spherical AuNP, PdNP and Fe_2O_3NPs, but the effect of Fe_2O_3 NP shape was also investigated.

Plasmonic heating is a method of heating materials that does not involve directly heating the bulk solution, but the NPs themselves (Figure α). Plasmonic heating is a process that makes use of optical properties that arise from localized surface plasmon resonance (LSPR) of a NP; plasmonic behavior is due to coherent oscillation of electrons in the conduction band in resonance with light of a particular

frequency.[x] The plasmon band of NPs is tunable, and is highly dependent on the NPs size, shape, and composition.[x] During plasmonic heating, visible or near-infrared (NIR) light is converted to heat through nonradiative relaxation of the excited LSPR; this can be achieved through electron-electron, electron-phonon (a non-conserved quantum of lattice vibration), and phonon-phonon interactions.[x,y] Thus, the nanoparticles are heated through the use of light rather than through bulk heating (Figure α). Currently there are no direct methods of measuring the temperature of nanomaterials plasmonically heated; only predictions have been made through plasmonically heating AuNPs suspended in ice.[cc] Due to AuNPs emerging use in photothermal therapy, it is of interest to devise a way to determine the temperature at the surface of a NP; the heat generated by the NP is directly used to destroy tumor cells.[cc]

Due to the direct heating of the NP itself, the temperature of the NP surface cannot be measured by simply measuring the temperature of the bulk solution, as the temperature of the NP surface and the solution are not the same (Figure α). In an effort to develop a method of measuring local temperatures, we have assessed the use of multifunctional nanoparticles of different compositions. In this research, DNA functionalized Au-Fe_2O_3, Pd-Fe_2O_3, and Au-Pd-Fe_2O_3 NPs were used to monitor the temperature at the NPs surface through DNA melting temperature. While this report focuses primarily on the ability of one type of DNA strand to be functionalized to a NP and be used as a nanothermometer, the overall goal is to create a multiplex nanostructure, a NP with many different DNAs attached, in order to assess a wide array of temperatures on the surface of various NPs.[i]

The design of these nanothermometers begins with a stem loop (SL) DNA molecule. SL DNA contains a self-complementary region known as the "stem", as well as a "loop" of unpaired nucleotides (nts). SL DNA can be "melted", to form single stranded DNA; this occurs at a predictable temperature, the melting temperature (T_m). The T_m is a temperature that is specific to the sequence of a particular SL, and can be modified by changing the length of the stem and loop, changing the ratio of A-T and G-C bps, and introducing mismatch base pairs. In a nanothermometer, the DNA is modified on both ends: one end being thiolated and the other end containing a fluorescent molecule. This bifunctional DNA is attached to the surface of Au or Pd NP through an Au-S or Pd-S linkage while the fluorophore present at the other is

used to further probe the environment.[o,d,g] It has been previously reported that the fluorescence of the fluorophore is quenched when within close proximity to an AuNP surface (>5nm) through nanometal surface energy transfer (NSET). To the best of our best knowledge we cannot find this being described with Pd based NPs.[g]

When starting at a low temperature, all of the DNA molecules will be in the closed, quenched form. As the temperature increases towards the DNA's melting temperature, the DNA begins to unfold in a predictable manner, which is based on its T_m. Fluorescence should thus increase sharply around the T_m, when the fluorophore moves away from the quenching vicinity of the NP, exhibiting a sigmoidal rise in intensity as the temperature is increased; this can then be observed using fluorescence spectroscopy (Figure o).

Experimental

Materials. Tris(2-carboxyethyl)phosphine hydrochloride (TCEP), sodium acetate buffer solution, phosphate buffer solution (PBS), sodium dodecyl sulfate (SDS) solution, Tris-EDTA buffer solution, sodium chloride, sodium citrate tribasic dihydrate, gold(III) chloride trihydrate ($HAuCl_4$), iron(III) oxide, and concentrated nitric and hydrochloric acid were purchased from Sigma-Aldrich. All oligonucleotides were purchased from Sigma-Aldrich and were used as received.

NP synthesis. Gold spherical nanoparticles were prepared by a citrate reduction approach as reported earlier by our group. Specifically, 1.25×10^{-4} M Au^{3+} was heated to boiling and 1% (w/v) sodium citrate solution was added. The boiling was continued until the solution turned ruby red, indicating the formation of gold nanoparticles. The resulting nanoparticles were purified by centrifugation and re-dispersion in deionized (DI) water. Pd NPs were produced in the same manner, replacing Au^{3+} with Pd^{2+}.

Au-Fe_2O_3 NPs (or Pd-Fe_2O_3 NPs) were synthesized by first combining 10 µL of a 25 mM Fe_2O_3 NP stock with 10 mL DI water, and heating with stirring for 5 minutes. Then 1 mL of a 1% (w/v) sodium citrate solution was added and the mixture was brought to a boil. Then 250 µL of a 0.01 M $HAuCl_4$ (or 250 µL 0.01 M H_2PdCl_4 in the case of Pd-Fe_2O_3) solution was added and the mixture was heated with

stirring at 100°C for 10 minutes. The resulting suspension was then cooled and purified by centrifugation, and re-dispersed in DI water.

Au-Pd-Fe_2O_3 NPs were synthesized by first adding 2 mL of an unwashed Au-Fe_2O_3 suspension and 4.5 mL DI water to a 25 mL Erlenmeyer flask. Then, 0.5 mL of 0.1 M ascorbic acid was added, followed by a stepwise addition of 8.6 μL of 0.01 M H_2PdCl_4 every 5 minutes until 86 μL has been added. The mixture was then stirred for 30 minutes at room temperature to complete the reaction. The particles were then purified by centrifugation.

Nanothermometer synthesis. First, the disulfide bond of the thiolated DNAs was reduced overnight at room temperature in the presence of freshly prepared 0.1 M TCEP and 0.5 M sodium Acetate buffer (pH 5.2). Next, solutions of freshly activated thiol modified DNA and oligoT helper strand (Table 1) were then added to 1000 μL suspension of NP's in 10 mM phosphate buffer (pH 7.7) containing 0.01% (v/v) SDS. The final concentrations of the DNA and helper strand were 2 μM and 1 μM, respectively. To allow self-assembly of the DNAs through the formation of an Au-S or Pd-S bond, the DNA, helper strand and NP were incubated at room temperature for 25 min with gentle shaking. To ensure maximal loading of DNA to the NP, the concentration of sodium chloride was then increased step-wise using a 2.0 M stock solution, in increments of 50 μL until a concentration of 1.0 M was achieved.[n] The mixture was then incubated with gentle shaking for 12 hours at ambient temperature between each addition of salt. Upon completion of the salt aging step, the mixture was incubated overnight at room temperature. Excess oligos were removed by centrifuging the mixture at 9,000 rpm for 7 minutes at 10°C. The mixture was then washed three times with 0.01% SDS, and the precipitate was finally dispersed into 1000 μL of measurement buffer (0.3 M NaCl, 10 mM PBS, pH 7.7).

Fluorescence Measurements. Fluorescence measurements were performed using a Cary Eclipse fluorescence spectrophotometer. Texas Red, FAM and Pacific Blue were excited at 583, 495 and 395 nm respectively, and the fluorescence emission spectra were collected from 590-800 nm, 500-700 nm and 405-600 nm, respectively. The nanothermometers were suspended in measurement buffer (0.3 M NaCl, 10 mM PBS, pH 7.7) and heated via a water bath. Measurements were collected with at least 1 mL

sample volume in 1.00 cm path length plastic cuvettes from 10-80°C. Excitation and emission slit widths of 5-10 nm were used (as recorded). Melting curves of the NP-DNA conjugates were obtained by plotting the fluorescence intensity at the maximum wavelength against the temperature of the measurement.

Scanning Electron Microscopy. Nanothermometers were imaged with scanning electron microscopy and energy dispersive x-ray spectroscopy using a Hitachi SU8230 Scanning Electron Microscope. The nanothermometers were washed with pure water to remove NaCl; then 10 μL was placed on Carbon Type-B 400 Mesh Copper Grids and allowed to dry for several hours at room temperature. Images were acquired at 15 kV and a working distance of 10 mm.

ζ-potential measurements. The ζ-size and ζ-potential was determined for all NPs and NP-DNA conjugates through dynamic light scattering (DLS) and phase analysis light scattering (PALS), using a NanoBrook Omni Zeta Potential Analyzer. It was determined that in order to prepare dust free samples suitable for light scattering measurements, 15 mL of measurement buffer must be filtered three times through an Acrodisc® 25 mm Syringe Filter with 0.45 μm Versapor® membrane, and added to a 15 mL conical tube that has been rinsed three times with filtered water. Then, wasting the first two drops of NP suspension, a third drop of NPs was added to the filtered measurement buffer. A 1.00 cm path length plastic cuvette was rinsed with the dilute sample three times, sonicating the cuvette for at least 15 seconds during each wash. Finally, all measurements were recorded at 25.00°C.

Results and Discussion

Stem Loop DNA Design. The initial purpose of this study was to assess the ability of Au-Fe_2O_3, Pd, Pd-Fe_2O_3, and Au-Pd-Fe_2O_3 nanoparticles to be used as nanothermometers. Three different SLs and a spacer oligo (a short DNA) were used (Figure β).[i] In order to increase the temperature range of these nanothermometers, two additional oligos were designed using web based tools. As our target thermometry range is much higher than that of the previously reported nanothermometers (>100°C, in order to measure the surface temperature of the AuNP when subjected to plasmonic heating), we chose target melting points of 80 and 100°C in the design of the corresponding SLs.

AuNPs are most efficient at quenching the fluorophore at distances of less than 5 nm, so the SLs were designed in a manner such that the fluorophore does not exceed this distance from the NP when the SL is in the closed form (has complementary base pairing, forming a "stem") and the fluorophore sufficiently exceeded this distance from the NP when in the open form (the DNA is now single stranded).[g,h,i] To do this, SLs were designed to have rather long stems, a factor that fortunately inherently increases the stability of the SL (as well as the high G-C content).

Our goal was to design more stable SLs with high T_m's, so a G-C rich stem was used. In order to increase the length of the SL an external single stranded region of DNA was added; this consisted of a string of ten thymines, as they have the lowest tendency to be adsorbed on the surface of AuNP.[f,i]

Using these strategies and the help of Integrated DNA Technologies OligoAnalyzer 3.1 online tool, many potential structures were designed, and their optimum secondary structures (Figure β) and corresponding thermodynamic properties were predicted for the proposed experimental conditions (0.3 M NaCl, 10 mM PBS, pH 7.7). First, a SL with a stem of 25 G-C bps and a loop of 3 nts (ATA) was used (Oligo100). Oligo100 had a predicted T_m of ~100°C under the proposed experimental conditions. Then, while decreasing the stem, the size of the loop was increased to 13 nts, and every other G-C bp in the stem was changed to an A-T bp. This SL had a predicted T_m of ~80°C under proposed experimental conditions. Both of these SLs only had one predicted secondary structure, which is important because the presence of other secondary structures would lead to different (or multiple) T_m values.

Characterization of NPs and NP-DNA conjugates. The size and shape of the synthesized Au, Au-Fe_2O_3, Pd, Pd-Fe_2O_3, and Au-Pd-Fe_2O_3 NPs before and after their DNA functionalization were evaluated using scanning electron microscopy (SEM). Energy dispersive X-ray spectroscopy (EDS), a technique that measures characteristic X-rays to provide localized elemental information, was used concurrently with the SEM to give characteristic elemental data at localized points on the micrograph.[p] Nitrogens Kα emission at 397 eV was detected using EDS, and used to evaluate the presence DNA on the nanoparticles, as the NPs themselves do not contain nitrogen, nor does the copper grid the nanoparticles are imaged on.[dd]

The amount of sulfur was determined to be too low to be used to detect the presence of DNA on the nanoparticles (the presence of which was confirmed with fluorescence spectroscopy).

The size of all NPs before and after functionalization was additionally assessed using a dynamic light scattering (DLS). DLS measures the hydrodynamic radius of particles in a solution or suspension by measuring the random changes in intensity of light scattered.[q] The Stokes-Einstein equation models Brownian motion of small particles and can be used to determine particle size (at low concentration)[r]:

$$D_h = \frac{k_B T}{3\pi\eta D_t}, \tag{1.1}$$

where D_h is the hydrodynamic diameter, D_t is the translational diffusion coefficient, k_B is Boltzmann's constant, η is dynamic viscosity, and T is the absolute temperature.[r] Upon DNA functionalization of the NP, we expect that the hydrodynamic radius would increase fairly dramatically due to the presence of the DNA ligand.

The zeta potential is a measurement that represents electric potential at the slipping plane (between the Stern layer and diffuse layer of ions surrounding the particle) of the dielectric layer in colloids. The zeta potential was determined for all NPs and NP-DNA conjugates were assessed using phase analysis light scattering (PALS). PALS measures the phase shift in light (when compared to a reference beam) that is scattered from particles in a suspension in which an electric field has been applied.[k] The zeta potential gives an indication of stability of particles, as particles with a largely positive or negative zeta potential (> +30 mV or < -30 mV) tend to repel each other and do not tend to flocculate.[k] Zeta potential is highly dependent on a particle's immediate environment, including pH and ionic strength.[j] For this reason, all measurements were taken under the same conditions (0.3 M NaCl, 10 mM PBS, 25.00 °C).

To determine the zeta potential, the phase shift is measured, and can be used to determine the particles electrophoretic mobility, which can then be used to calculated zeta potential using Smoluchowski's equation[k]:

$$\mu_e = (4\pi\varepsilon_0) \cdot \frac{D\zeta}{4\pi\eta} = \frac{\varepsilon\zeta}{\eta}, \tag{1.2}$$

where μ_e is the electrophoretic mobility, ε is electrical permittivity, ε_0 is the permittivity of free space, $D = \frac{\varepsilon}{\varepsilon_0}$, and ζ is the zeta potential.

When a ligand, such as the SL, is added to the surface of a NP, zeta potential calculations become complex due to the change in hydrodynamic size and surface charge shield that is dependent on the conformation of the DNA (whether it is in the SL or single stranded form). Fortunately we believe the change in surface potential due to the change in surface functionalities can be used as a qualitative method to evaluate successful functionalization of the DNA to the NP.[j] The nanoparticles used in this study were synthesized and capped with various surfactants (citrate, aspartate, etc), which were displaced by DNA molecules, resulting in a change in magnitude of the zeta potential of functionalized NPs (Figure a).[j] In the case of Au, Pd, and Au-Pd-Fe_2O_3 NPs, a significant increase in the zeta potential is observed after the addition of the SL. In the case of the Pd-Fe_2O_3 (spheres, rings and tubes), no obvious correlation between the zeta potential before and after the addition of the DNA is observed (Table b). This could be due to the original ligand on the surface of the Fe_2O_3 portion of the NPs, and is currently under investigation.

The NPs and NP-DNA conjugates optical properties were evaluated via UV-Vis spectroscopy. Size and shape of NPs affects their optical properties, specifically localized surface plasmon resonance (LSPR) wavelengths, which can be observed as large peaks in either the visible or NIR region of the spectrum[a,b]. For AuNPs, these properties have been widely characterized and visible spectroscopy can be used to determine the size and concentration of AuNPs.[l] Unfortunately, analysis of the optical properties of Pd, Au-Pd-Fe_2O_3 and Au-Fe_2O_3 is less prevalent, and thus lacking each particle's specific extinction coefficients, the concentration of the NPs used in this study was not determined. AuNPs exhibit LSPR, which is dependent on the size and shape of the NPs. In AuNPs, the LSPR wavelength can be tuned by varying the size between 1-100 nm.[l] Pd lacks any characteristic peaks in the UV-Vis spectrum, though it has been reported to also potentially exhibit plasmonic properties.[m] Fe_2O_3 NPs absorb strongly in the UV

region and this was used to confirm its presence. Additionally, the success of DNA conjugation to a NP can be monitored with UV spectroscopy, making use of DNA's absorbance at 260 nm (Figure i).

The NP-DNA conjugate's ability to function as a nanothermometer was assessed using fluorescence spectroscopy. Each NP-DNA conjugate was excited at the fluorophore's specific excitation wavelength and the emission spectra of the fluorophores were recorded while bulk heating was applied to the solution. The maximum emission wavelength was plotted against temperature and did not result in a sigmoidal shape (as expected) as a result of the temperature increase, which could be the result of many factors, including the experimental set-up as well as the unknown properties of the interactions between the NP and the fluorophore. In the case of Au-Pd-Fe_2O_3-DNA conjugates, a linear increase in fluorescence with increased temperature was observed (Figure c). These results are highly reproducible as three measurements of three separately prepared NP-DNA conjugates were recorded. Due to the high reproducibility of the melting curves produced by the Au-Pd-Fe_2O_3 NPs-DNA conjugates, these appear to be our best nanothermometer candidate.

No significant trend is observed in Pd, Pd-Fe_2O_3 or Au-Fe_2O_3 NP-DNA conjugates (Figure b, e, h), which can possibly be attributed to our lack of the ability to control the temperature as the measurements were being recorded, or possibly that the properties of the NPs used actually allowed for enhancement of the fluorophore rather than quenching.[s]

Conclusion

A straightforward approach was developed for the synthesis of Pd, Pd-Fe_2O_3, Au-Fe_2O_3, and Au-Pd-Fe_2O_3 nanothermometers, using a single SL DNA. These NP-DNA conjugates were characterized using techniques including EDX measurements, ζ-potential of NPs before and after DNA functionalization, electron microscopy studies and fluorescence spectroscopy. The fluorescence studies of the NP-DNA demonstrate the interaction between the NP and the fluorophore, which is quenched in the case of Au-Pd-Fe_2O_3 NPs and is perhaps enhanced (when compared to AuNPs) in the case of Pd and Pd-Fe_2O_3 NPs. In order to achieve more accurate and reproducible measurements, designing a system that is able to hold the NP-DNA conjugates at a temperature for a longer period of time to allow them to

equilibrate is currently underway. Our studies show that Au-Pd-Fe_2O_3 NPs are the best candidate material to serve as nanothermometers when compared to Pd, Pd-Fe_2O_3, and Au-Fe_2O_3 materials.

References

a. Heiligtag, F. J.; Niederberger, M. The Fascinating World of Nanoparticle Research. *Materials Today*. **2013**, *16*, 262–271.
b. Giljohann, D. A.; Dwight S. Seferos, D. S.; Daniel, W. L.; Massich, M. D.; Patel, P. C.; Mirkin, C. A. Gold Nanoparticles For Biology and Medicine. *Angewandte Chemie International Edition*. **2010**, 3280–3294.
c. Chou, L. Y. T.; Zagorovsky, K.; Chan, W. C. W. DNA Assembly of Nanoparticle Superstructures for Controlled Biological Delivery and Elimination. *Nature Nanotech Nature Nanotechnology*. **2014**, *9*, 148–155.
d. Elghanian, R. Selective Colorimetric Detection of Polynucleotides Based on the Distance-Dependent Optical Properties of Gold Nanoparticles. *Science*. **1997**, *277*, 1078–1081.
e. Adams, B. D.; Chen, A. The Role of Palladium in a Hydrogen Economy. *Materials Today*. **2011**, *14*, 282–289.
f. Demers, L. M.; Mirkin, C. A.; Mucic, R. C.; Reynolds, R. A.; Letsinger, R. L.; Elghanian, R.; Viswanadham, G. A Fluorescence-Based Method For Determining the Surface Coverage and Hybridization Efficiency of Thiol-Capped Oligonucleotides Bound to Gold Thin Films and Nanoparticles. *Analytical Chemistry Anal. Chem.* **2000**, *72*, 5535–5541.
g. Machleidt, T.; Woodroofe, C. C.; Schwinn, M. K.; Méndez, J.; Robers, M. B.; Zimmerman, K.; Otto, P.; Daniels, D. L.; Kirkland, T. A.; Wood, K. V. NanoBRET—A Novel BRET Platform For the Analysis of Protein–Protein Interactions. *ACS Chem. Biol. ACS Chemical Biology*. **2015**, *10*, 1797–1804.
h. Algar, W. R.; Massey, M.; Krull, U. J. The Application of Quantum Dots, Gold Nanoparticles and Molecular Switches to Optical Nucleic-Acid Diagnostics. *TrAC Trends in Analytical Chemistry*. **2009**, *28*, 292–306.
i. Ebrahimi, S.; Akhlaghi, Y.; Kompany-Zareh, M.; Rinnan, Å. Nucleic Acid Based Fluorescent Nanothermometers. *ACS Nano*. **2014**, *8*, 10372–10382.
j. Doane, T. L.; Chuang, C.-H.; Hill, R. J.; Burda, C. Nanoparticle ζ -Potentials. *Accounts of Chemical Research Acc. Chem. Res.* **2012**, *45*, 317–326.
k. Hunter, R. J. *Zeta Potential in Colloid Science. Principles and Applications*; Academic Press: London, 1981.
l. Haiss, W.; Thanh, N. T. K.; Aveyard, J.; Fernig, D. G. Determination Of Size and Concentration of Gold Nanoparticles from UV−Vis Spectra. *Analytical Chemistry Anal. Chem.* **2007**, *79*, 4215–4221.
m. Lu, X.; Rycenga, M.; Skrabalak, S. E.; Wiley, B.; Xia, Y. Chemical Synthesis Of Novel Plasmonic Nanoparticles. *Annual Review of Physical Chemistry Annu. Rev. Phys. Chem.* **2009**, *60*, 167–192.
n. Hurst, S. J.; Lytton-Jean, A. K. R.; Mirkin, C. A. Maximizing DNA Loading On a Range of Gold Nanoparticle Sizes. *Analytical Chemistry Anal. Chem.* **2006**, *78*, 8313–8318.
o. Love, J. C.; Wolfe, D. B.; Haasch, R.; Chabinyc, M. L.; Paul, K. E.; Whitesides, G. M.; Nuzzo, R. G. Formation And Structure of Self-Assembled Monolayers of Alkanethiolates on Palladium. *J. Am. Chem. Soc. Journal of the American Chemical Society*. **2003**, *125*, 2597–2609.
p. Hafner, B. Energy Dispersive Spectroscopy On the SEM: A Primer. Characterization Facility, University of Minnesota: Twin Cities.
q. Nanocompsix's Guide To Dynamic Light Scattering Measurement and Analysis **2012**.
r. Ekemezie, P. N.; Nwadiogbu, J. O.; Enekwechi, E. E. Determination Of the Diffusion Coefficient of Sucrose in Water and Its Hydrodynamic Radius. *Der Pharma Chemica*. **2015**.
s. Yun, C. S.; Javier, A.; Jennings, T.; Fisher, M.; Hira, S.; Peterson, S.; Hopkins, B.; Reich, N. O.; Strouse, G. F. Nanometal Surface Energy Transfer In Optical Rulers, Breaking the FRET Barrier. *J. Am. Chem. Soc. Journal of the American Chemical Society*. **2005**, *127*, 3115–3119.

t. Her, S.; Jaffray, D. A.; Allen, C. Gold Nanoparticles for Applications in Cancer Radiotherapy: Mechanisms and Recent Advancements. *Advanced Drug Delivery Reviews*. **2015**.
u. Chen, R.; Huang, X.; Xu, H.; Xiong, Y.; Li, Y. Plasmonic Enzyme-Linked Immunosorbent Assay Using Nanospherical Brushes As a Catalase Container for Colorimetric Detection of Ultralow Concentrations of Listeria Monocytogenes. *ACS Appl. Mater. Interfaces ACS Applied Materials & Interfaces*. **2015**, *7*, 28632–28639.
v. Freedman, K. J.; Bastian, A. R.; Chaiken, I.; Kim, M. J. HIV Detection: Solid-State Nanopore Detection Of Protein Complexes: Applications in Healthcare and Protein Kinetics (Small 5/2013). *Small*. **2013**, *9*, 645–645.
w. Lukianova-Hleb, E. Y.; Kim, Y.-S.; Belatsarkouski, I.; Gillenwater, A. M.; O'neill, B. E.; Lapotko, D. O. Intraoperative Diagnostics and Elimination of Residual Microtumours with Plasmonic Nanobubbles. *Nature Nanotech Nature Nanotechnology*. **2016**.
x. Aioub, M.; El-Sayed, M. A. A Real-Time Surface Enhanced Raman Spectroscopy Study Of Plasmonic Photothermal Cell Death Using Targeted Gold Nanoparticles. *J. Am. Chem. Soc. Journal of the American Chemical Society*. **2016**, *138*, 1258–1264.
y. Brongersma, M. L.; Halas, N. J.; Nordlander, P. Plasmon-Induced Hot Carrier Science and Technology. *Nature Nanotech Nature Nanotechnology*. **2015**, *10*, 25–34.
z. Hainfeld, J.; H. Intravenous Magnetic Nanoparticle Cancer Hyperthermia. *International Journal of Nanomedicine IJN*. **2013**, 2521.
aa. Freestone, I.; Meeks, N.; Sax, M.; Higgitt, C. The Lycurgus Cup — A Roman Nanotechnology. *Gold Bulletin Gold Bull*. **2007**, *40*, 270–277.
bb. Mody, V.; Siwale, R.; Singh, A.; Mody, H. Introduction To Metallic Nanoparticles. *Journal of Pharmacy and Bioallied Sciences J Pharm Bioall Sci*. **2010**, *2*, 282.
cc. Govorov, A. O.; Richardson, H. H. Generating Heat with Metal Nanoparticles. *Nano Today*. **2007**, *2*, 30–38. Harada, Y.; Takeuchi, T.; Kino, H.; Fukushima, A.; Takakura, K.; Hieda, K.; Nakao, A.; Shin, S.; Fukuyama, H. Electronic Structure Of DNA Nucleobases and Their Dinucleotides Explored by Soft X-Ray Spectroscopy. *J. Phys. Chem. A The Journal of Physical Chemistry A*. **2006**, *110*, 13227–13231.

OligoT Helper TTTTTTTTTT-$(CH_2)_3$-SH
OligoF FAM ATCATAATTATTGTTTTTTTTTTTTTTTACTATTTTTTTGAT-(10T)-$(CH_2)_3$-SH
OligoTR TR-ATCTAATCATTATTGTTTTTTTTTTTTTTTACTATTATGTTTAGAT-(10T)-$(CH_2)_3$-SH
OligoPB PB 425-ATATACATTTGTTTTTTTTTTTTACATATGTATAT-(10T)-$(CH_2)_3$-SH
*Oligo80 T*R-TGCGCGCGCCGCCGGCGGCCGCCGGCGATACGCCGGCGGCCGCCGGCGGCGCGCGC-(10T)-$(CH_2)_3$-SH
Oligo100 FLC-TGCACTCGCTGTCGGAGGCTGCTATATATAATATAGCAGCCTCCGACAGCGAGTGC-(10T)-$(CH_2)_3$-SH

Table 1. Sequences of oligonucleotides used in this study.

	ζ Potential of NP (mV)	ζ Potential of NP-DNA conjugate (mV)
20 nm Au spheres		
$AuFe_2O_3$ Spheres	**-23±6**	
$PdFe_2O_3$ Spheres	**-23±7**	
$PdFe_2O_3$ Rings	**-11±4**	**-10±3**
$PdFe_2O_3$ Tubes	**-12±4**	**-14±4**
Pd	**-15±4**	**-10±6**
$AuPdFe_2O_3$	**-15±5**	**-11±3**

Table b. ζ potential of NPs and NP-DNA conjugates, all measurement were taken in measurement buffer (0.3 M NaCl, 10 mM phosphate buffer, pH 7.7) at 25.00℃. All values were determined using the Smoluchowski approxiation.

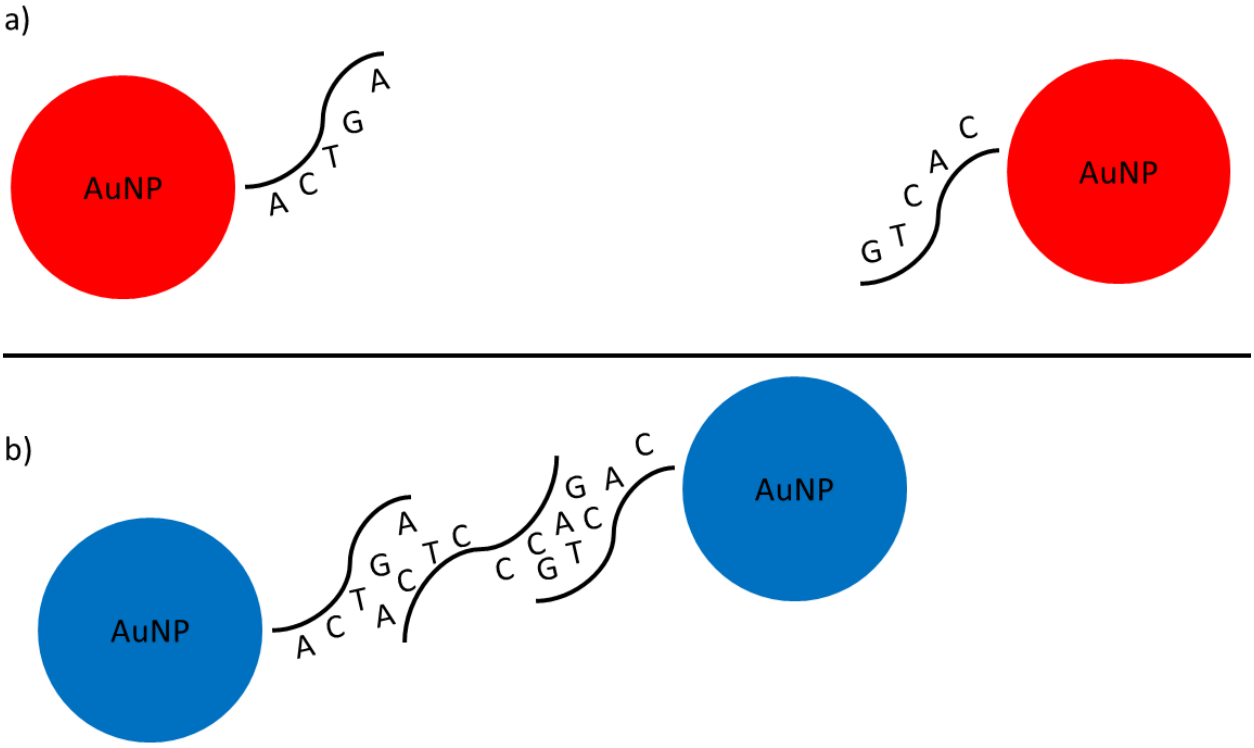

Figure κ. The original experiment performed by Mirkin et al. involved the addition of two non-complementary DNAs to be attached to AuNPs, resulting in a red solution. These were unable to form complementary base pairs with each other, so when combined the solution still remained red. However, when a third DNA (not conjugated to an AuNP) was added, that was able to bring the other NPs together through complementary base pairing, the solution immediately turned blue. The color change of this solution is reversible, through the addition of heat sufficient to disrupt the hydrogen bonding between base pairing.

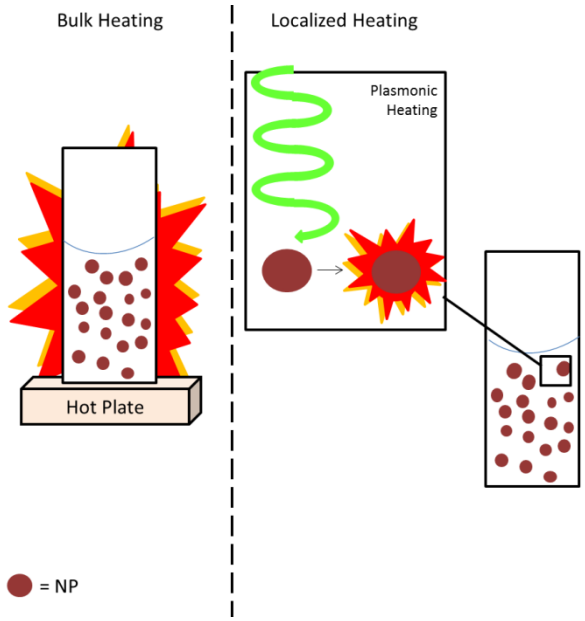

Figure α. Bulk heating of NPs can be achieved simply through the use of a hot plate, or the direct use of heat to raise the temperature of the NPs through raising the temperature of the entire solution. Localized heating can be achieved through plasmonic heating, where visible or NIR light is converted to heat through nonradiative relaxation of the excited LSPR.

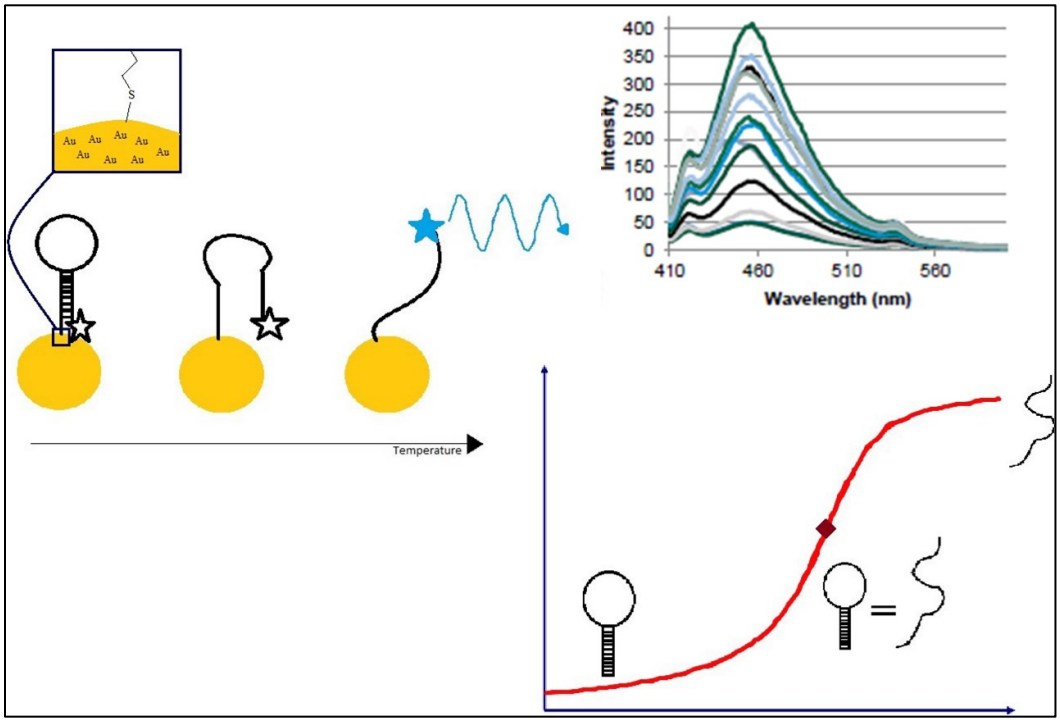

Figure o. Schematic diagram of the basic idea of nanothermometer function. A alkylthiol modified SL is attached to a Au or Pd NP through either a Au-S or Pd-S bond. As the NP-DNA are heated in solution, the DNAs begin to unfold in a fashion related to their stability, or T_m. As the DNA unfolds, the fluorophore is moved outside of the quenching vicinity of the NP, resulting in an increase in fluorescence that can be monitered using fluoresence spectroscopy.

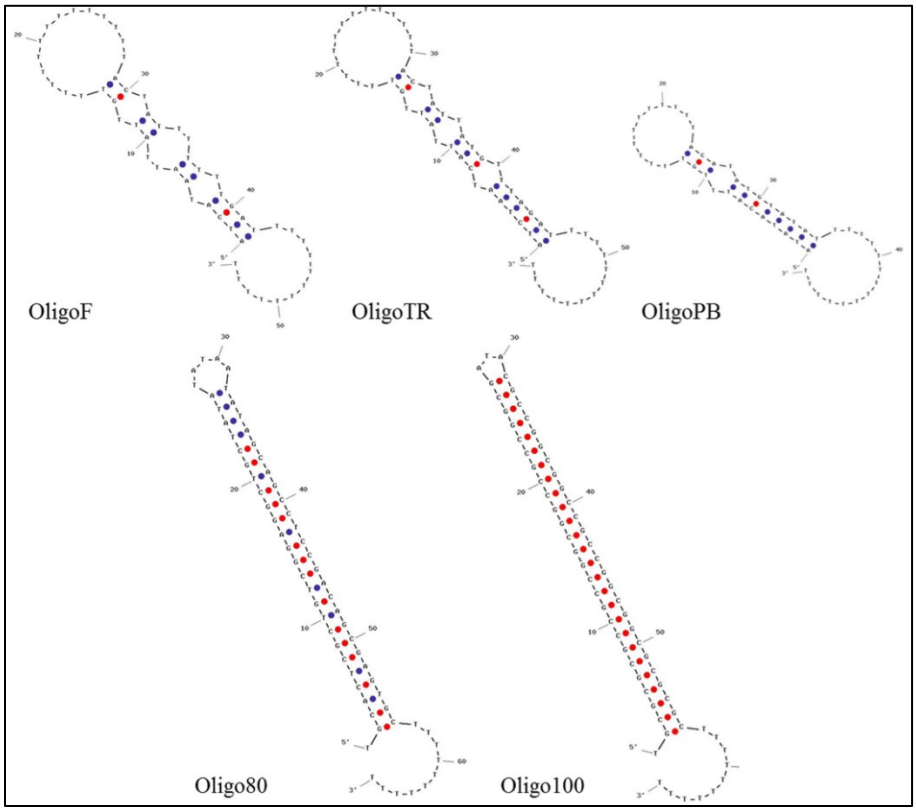

Figure β. Secondary structures of oligonucleotides used in this study under optimal experimental conditions (0.3 M NaCl, pH 7.7) generated using IDTs OligoAnalyzer.

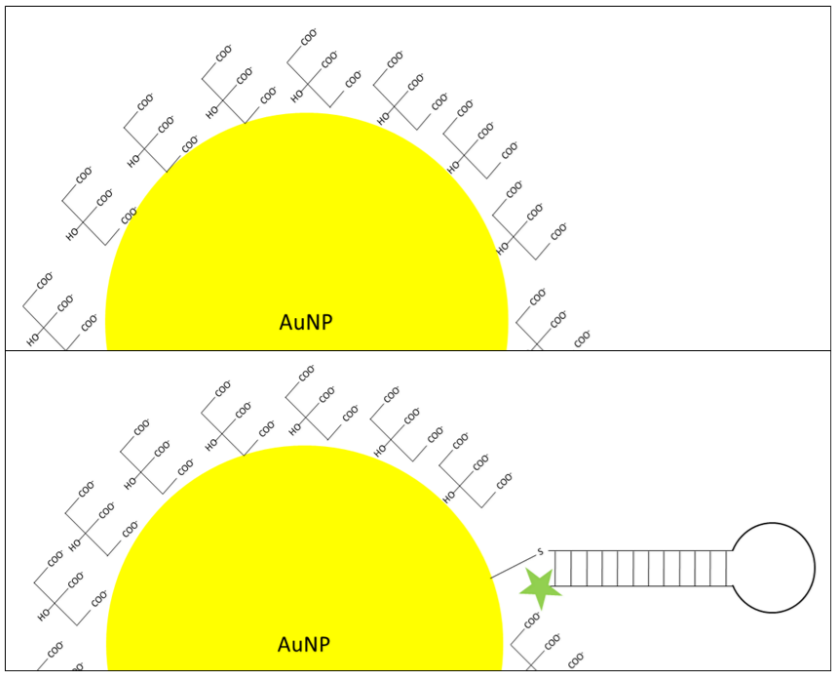

Figure a. Citrate capped AuNP with and without DNA functionalization. After DNA functionalization, some of the citrate cap has been replaced by SLs, thereby lowering the potential at the slipping plane (zeta potential).

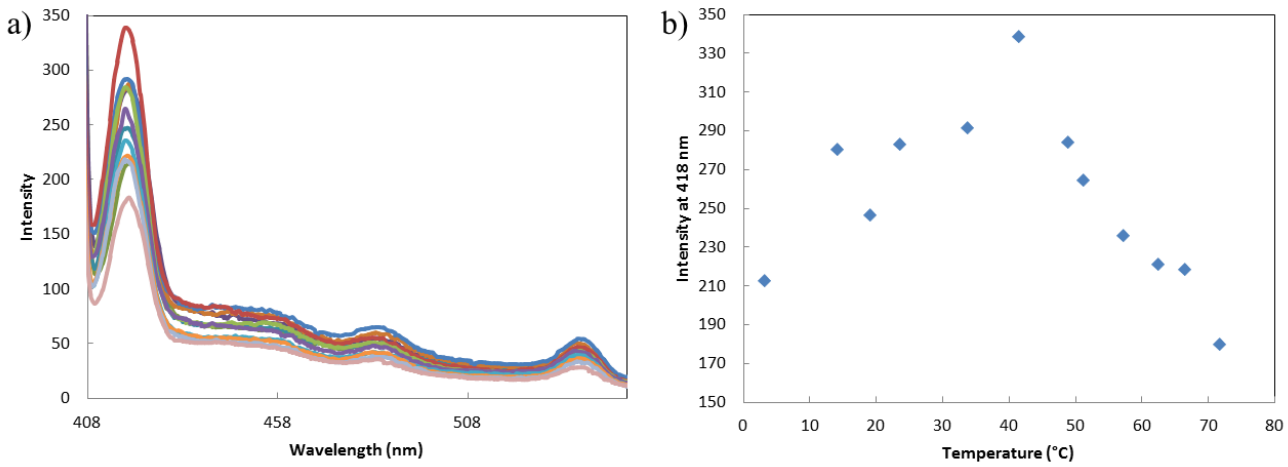

Figure b. a) Fluorescence emission spectra of AuFe2O3 Nanosphere OligoPB as temperature rises. An excitation energy of 395 nm was used. The excitation slit width was 5 nm and the emission slit width was 10 nm. b) Intensity of fluoresence of AuFe2O3 Nanosphere OligoPB at 418 nm as a function of temperature. No correlation can be determined between quenching of fluorescence of OligoPB and temperature.

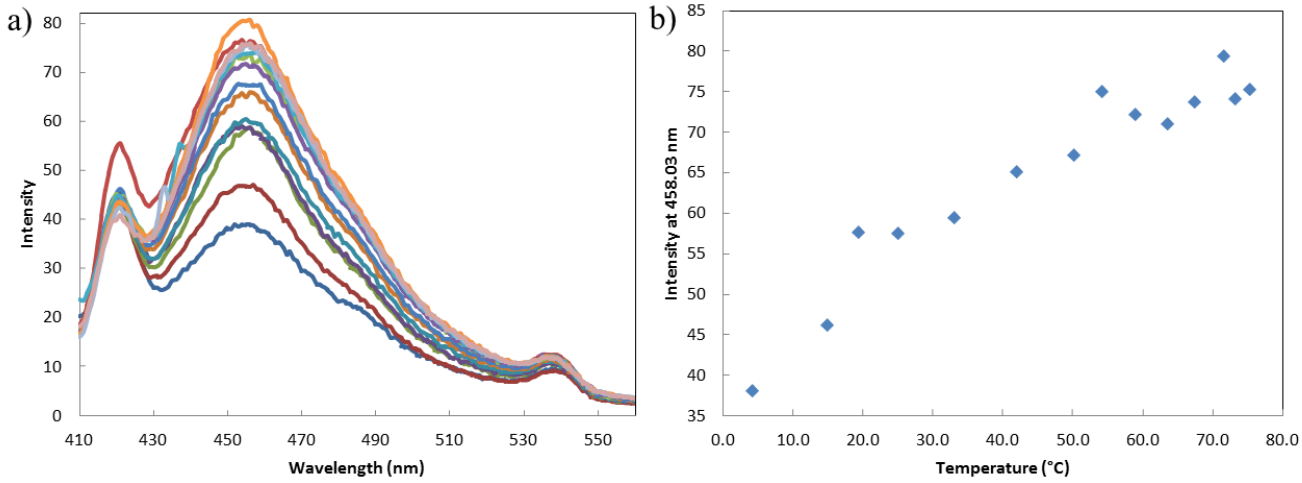

Figure c. a) Fluorescence emission spectra of AuPdFe2O3 Nanosphere OligoPB as temperature rises. An excitation energy of 395 nm was used. The excitation slit width was 5 nm and the emission slit width was 10 nm. b) Intensity of fluoresence of AuPdFe2O3 Nanosphere OligoPB at 458.03 nm as a function of temperature. A linear decrease in quenching of the fluorophore is observed as temperature is increased.

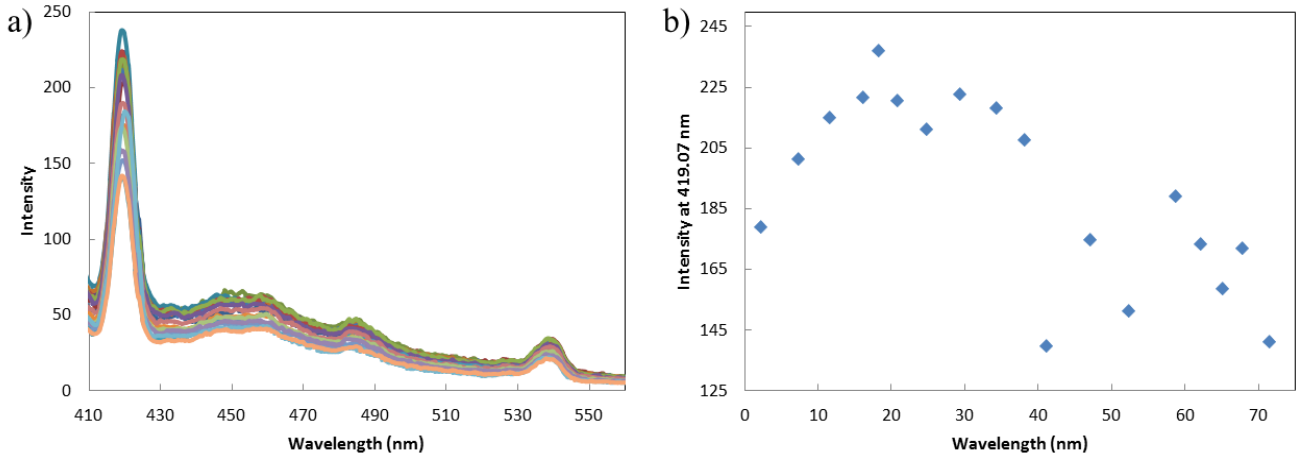

Figure e. a) Fluorescence emission spectra of PdFe2O3 Nanosphere OligoPB as temperature rises. An excitation energy of 395 nm was used. The excitation slit width was 5 nm and the emission slit width was 5 nm. b) Intensity of fluoresence of PdFe2O3 Nanosphere OligoPB at 419 nm as a function of temperature. An unexpected increase in quenching of the fluorophore is observed as temperature is increased.

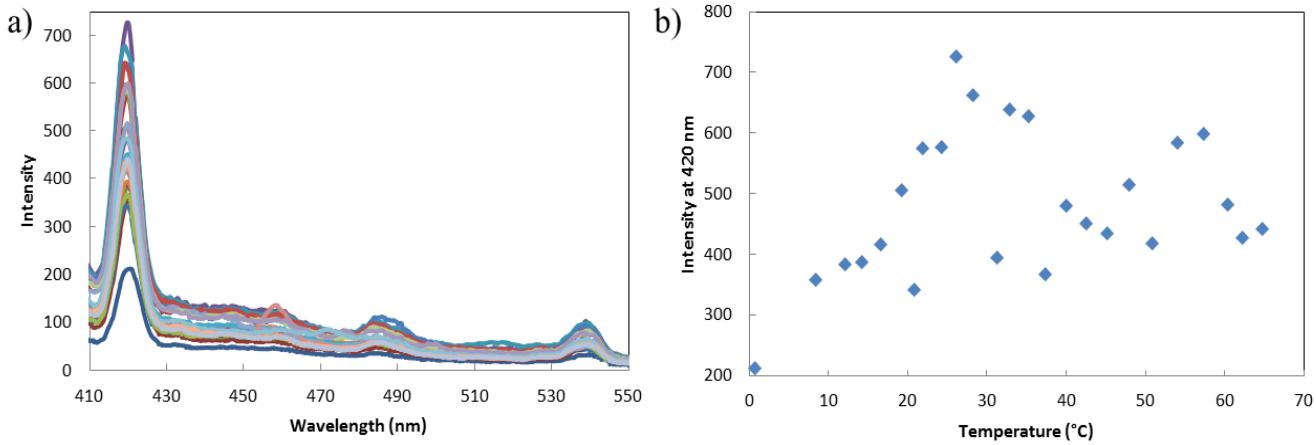

Figure h. a) Fluorescence emission spectra of Pd OligoPB as temperature rises. An excitation energy of 395 nm was used. The excitation slit width was 5 nm and the emission slit width was 5 nm. b) Intensity of fluoresence of Pd OligoPB at 420 nm as a function of temperature. No correlation can be determined between quenching of fluorescence of OligoPB and temperature.

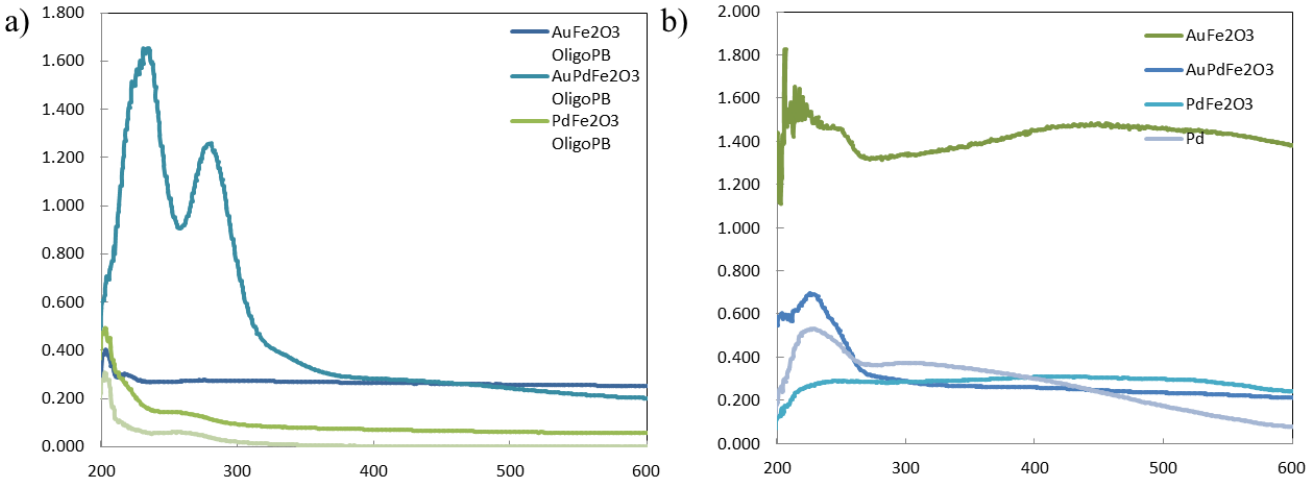

Figure i. a) UV-Vis spectra of all DNA functionalized (OligoPB) nanoparticles. b) UV-Vis spectra of all DNA functionalized (OligoPB) nanoparticles. All measurement were acquired in quartz cuvettes, pathlength 1.00 cm.

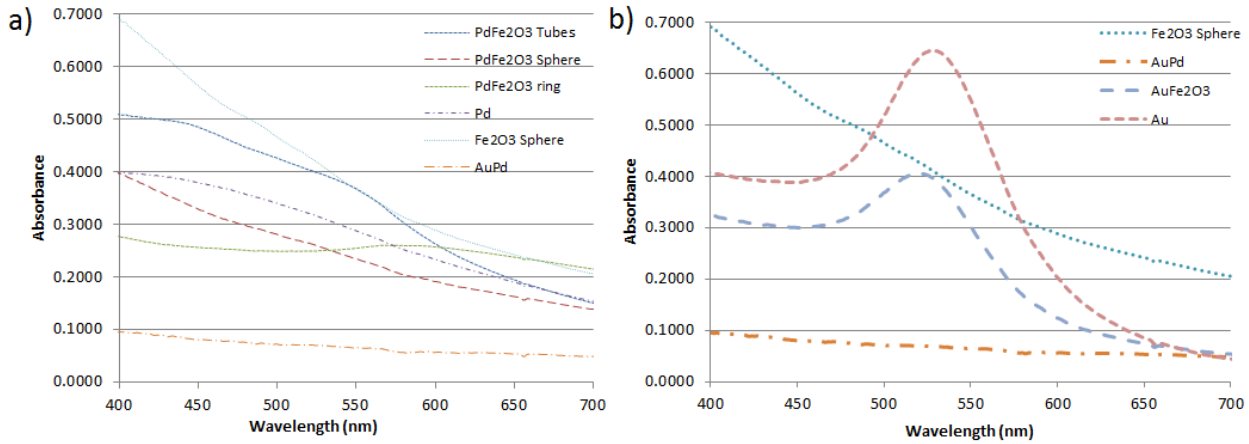

Figure j. a) UV-Vis spectra of all Pd NPs. b) UV-Vis spectra of all Au NPs. All measurement were acquired in quartz cuvettes, pathlength 1.00 cm

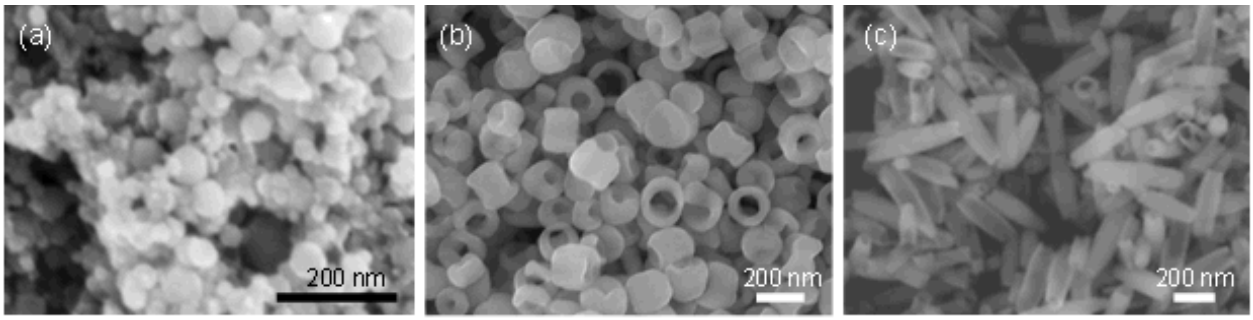

Figure o. SEM micrographs of a) Fe_2O_3 spheres, b) Fe_2O_3 rods, c) Fe_2O_3 tubes.